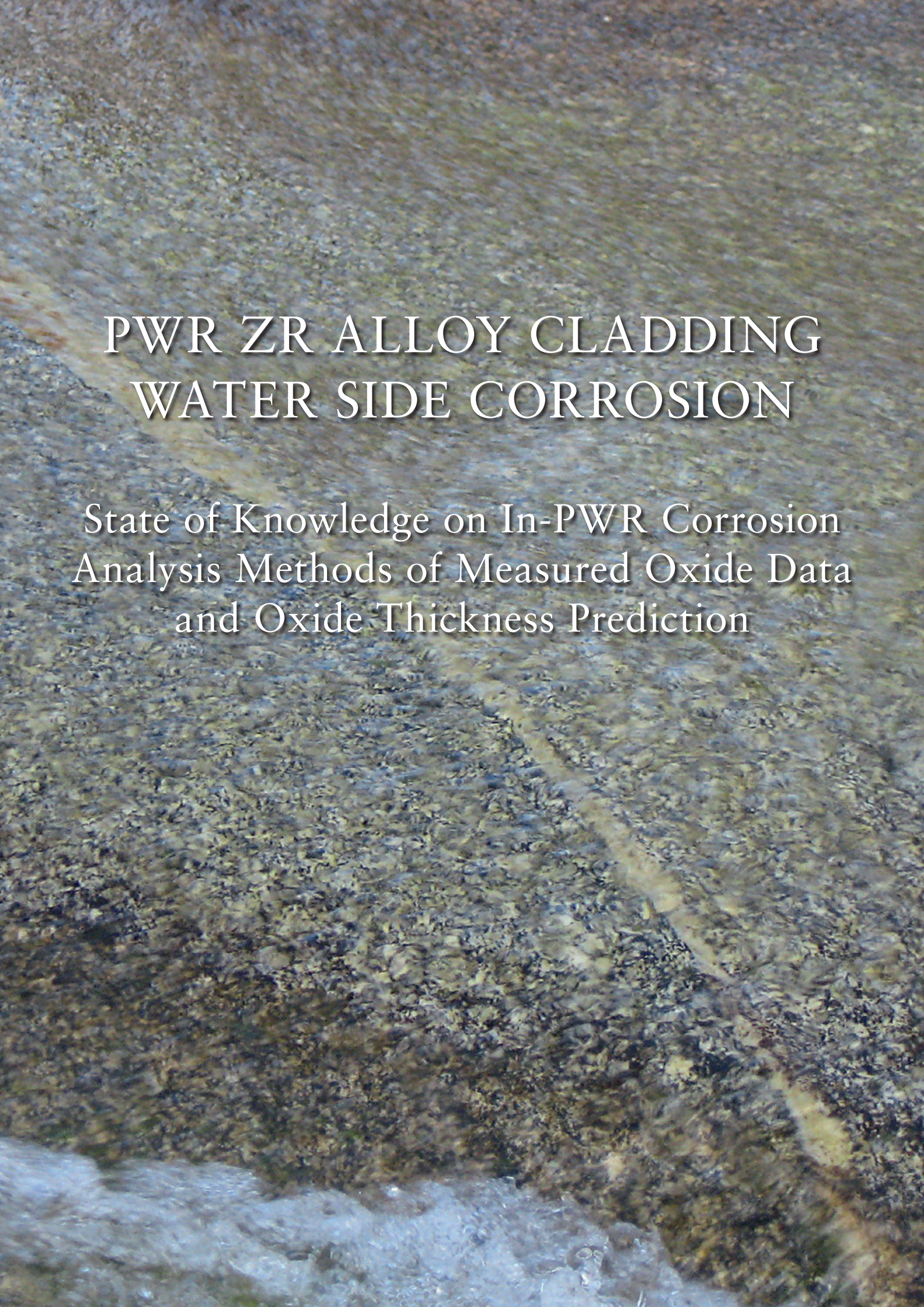

PWR ZR ALLOY CLADDING WATER SIDE CORROSION

State of Knowledge on In-PWR Corrosion Analysis Methods of Measured Oxide Data and Oxide Thickness Prediction

PWR Zr Alloy Cladding Water Side Corrosion

State of Knowledge on In-PWR Corrosion Analysis Methods of Measured Oxide Data and Oxide Thickness Prediction

Authors

Friedrich Garzarolli
Fürth, Germany

Matthias Garzarolli
Dresden, Germany

Editor

Peter Rudling
ANT International, Mölnlycke. Sweden

A.N.T. INTERNATIONAL®

© February 2012
Advanced Nuclear Technology International
Analysvägen 5, SE-435 33 Mölnlycke
Sweden

info@antinternational.com
www.antinternational.com

Ecolabelled printed matter, 441 799

Disclaimer

The information presented in this report has been compiled and analysed by Advanced Nuclear Technology International Europe AB (ANT International®) and its subcontractors. ANT International has exercised due diligence in this work, but does not warrant the accuracy or completeness of the information. ANT International does not assume any responsibility for any consequences as a result of the use of the information for any party, except a warranty for reasonable technical skill, which is limited to the amount paid for this Report.

Copyright © Advanced Nuclear Technology International Europe AB, ANT International, 2012.

Contents

Copyright © Advanced Nuclear Technology International Europe AB, ANT International, 2012.

1 Introduction

The entire area of corrosion (and the accompanying absorption of hydrogen in the zirconium metal matrix) is of prime interest when considering performance of the core components and therefore the performance of the entire reactor. For instance, a practical corrosion limit exists (for Pressurized Water Reactors (PWRs). The growth of oxide films on Zr-alloy Fuel Rod (FR) Claddings and Structural components has been treated extensively in the literature and the most important parameters impacting PWR corrosion rate are discussed in this Report, as follows:

- Temperature.
- exposure time,
- water chemistry, including impurities and Chalk River Unidentified Deposits (CRUD),
- neutron flux,
- Zr-alloy chemistry and condition,
- late acceleration of in PWR corrosion after formation of a dense hydride layer, irradiation induced dissolution of Second Phase Particles (SPP), or LiOH incorporation in the inner part of the oxide layer.
- Increase of corrosion or decrease of oxide thermal conductivity at high Burnups (Bus).

Corrosion of the Zr-alloy claddings and structural components proceeds quite different in the different reactor systems, such as PWR, Voda Voda Energo Reactor (Russian type PWR) (VVER), Boiling Water Reactor (BWR), Reaktor Bolshoi Mozhnosti Kanalov[1] (RBMK), Canadian Deuterium Uranium (CANDU), due to the different FR surface temperatures and water chemistry in the different types of power reactors. FR corrosion in PWRs is particularly affected by the thermo hydraulic characteristics of the PWR and the fuel duty. Therefore it is necessary to deduce corrosion constants from the measured oxide data that can be applied for predictions of the corrosion behaviour:

1) In the same reactor for an any power history or
2) in any other PWRs respectively.

The deduced corrosion constants can also allow a comparison of different material compositions and conditions for a future optimization of the Zr-alloys used for PWR fuel.

This Report describes and discusses the principle assumptions and constants, proposed in the literature for corrosion of Zr-alloy claddings in PWRs.

Furthermore an analytical model of measured oxide layers (Matthias-I) as well as a predictive model (Matthias-II) is described. The thermal hydraulic equations used to calculate the temperature and the corrosion equations governing the oxide layer build up are given together with the default numbers applied in the two codes. The default numbers can be changed, if desired. The program is written applying Microsoft Visual Basic 2010. An executable code version of the PWR FR oxide analysis program, Model that can be used on computers with Microsoft Windows XP or higher is provided together with this Report.

The described analysis tool is then used for an evaluation of literature oxide data. Finally conclusions are given on the effect of fuel clad chemical composition and conditions as much as possible from the published information.

In the Appendix the predictive model along with a User Manual for the PWR, FR oxide analysis program are provided. Also, the Appendix gives recommendations for various detailed analysis.

[1] In English Large Boiling Water Channel type reactor

Copyright © Advanced Nuclear Technology International Europe AB, ANT International, 2012.

2 In-PWR corrosion behaviour, principle assumptions and constants applied

2.1 Out-reactor corrosion and basic assumptions for in-PWR clad corrosion modelling

In most models the evaluation of the in-PWR corrosion is based on the out of reactor corrosion behaviour of Zr-alloys in oxygen free water. Out of reactor, in oxygen free water, the corrosion forms at first a dense protective oxide film. Initially, the corrosion kinetics in the temperature range on 250-400°C follows an approximate cubic law (Figure 2-1), the rate decreases with increasing oxide layer thickness, S, and time, t.

Eq. 2-1: $S^3=k\cdot t$

$S^3 = k\cdot t$

where

S is oxide layer thickness,

t is time, and

k is a constant.

At a certain thickness, the so called transition thickness (S_{Trans} = 1.5-3 µm) the oxide layer becomes porous causing a rate transition. After this transition, the corrosion rate is more or less constant and is governed by the thickness and quality of the innermost part of the oxide layer that controls the corrosion rate. This innermost part of the oxide layer is often called *barrier layer*. It should be mentioned, that the thickness of the barrier layer is always less than the total oxide thickness even in the pre-transition range, as Transmission Electron Microscopy (TEM) and penetration tests have shown.

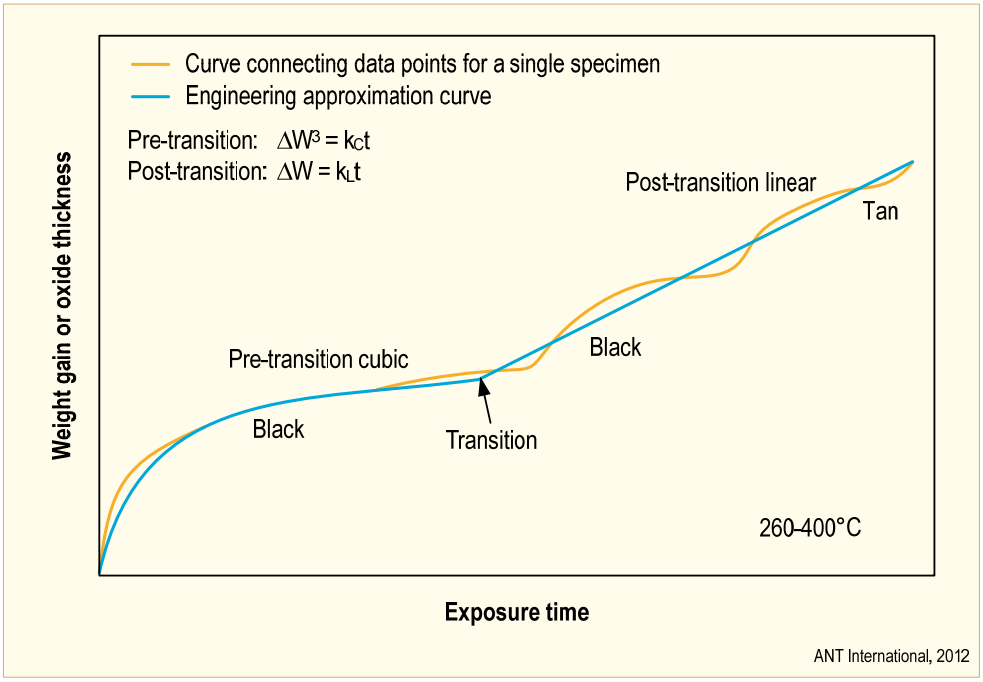

Figure 2-1: Schematic representation of the corrosion behaviour of Zircaloy (Zry)-4 in the temperature range 260-400°C, after [Hillner, 1977].

Copyright © Advanced Nuclear Technology International Europe AB, ANT International, 2012.

The corrosion rate (*ds/dt*) before and after the rate transition shows an exponential temperature dependence. For the post transition corrosion rate, which is most important for in-PWR corrosion modelling the following equation is used:

Eq. 2-2: $ds/dt = C. \exp(-Q/RT)$,

where

C is the corrosion constant that depends on Zr-alloy composition and final heat treatment condition,

Q is the activation energy,

R is the gas constant,

T is the absolute temperature.

The temperature effect on corrosion rate is related to the increased transport rate of the corrosion species responsible for the oxide growth (electrons and/or oxygen ions) with increased temperature. The activation temperature, Q/R, is reported to be between 11000 and 16000 K and appears to be quite independent of the Zr-alloy composition and final heat treatment condition.

This general model for the out-of-reactor corrosion process in oxygen free water is widely accepted, although it was pointed out, e.g. [Bryner, 1979], that the quasi-linear corrosion is in reality a periodic corrosion behaviour, repeating the first stage of oxide growth and transition at least at short to intermediate exposure times, see Figure 2-1.

A remarkable periodic repetition of certain features in oxide structure with distance from the metal/oxide interface was observed with different techniques, e.g. [Motta et al, 2006]. Optical microscopy and Scanning Electron Microscope (SEM) showed lateral cracks Figure 2-2 developed in the oxide with a certain periodicity. Also, variations of grain shape (columnar and equiaxed) X-ray peak intensities for both monoclinic and tetragonal zirconia, and texture were observed with distance form the metal/oxide interface.

The periodic repetition of lateral cracks was also observed for oxide formed in autoclave and in out of pile loops under a heat flux, and also for oxide layers formed in PWR at least for oxide thicknesses < 30 µm, e.g. [Bossis et al, 2006].

Considering the repeated corrosion rate transitions with time, see Figure 2-2, [Pêcheur et al, 2004] and [Bonieau et al, 2007] described in their model the corrosion behaviour with a cyclic behaviour of repeated corrosion rate transitions. Their model assumes the repetition of:

Eq. 2-3: Growth by diffusion: $ds^3/dt = k \cdot \exp(-Q/RT)$

until the oxide thickness reaches a thickness where a corrosion rate transition occurs:

$$s = s_{trans}$$

where

s = the oxide layer thickness in µm,

t is the time,

k is the corrosion constant (e.g. 6.92E9 for Zry-4[2] and M2[3],

s_{trans} is the transition thickness (e.g. 1.75 for Zry-4 and 2.08 for M2), and

Q/R is the activation temperature (e.g. 16.000 K).

[2] Zr1.5%Sn0.2%Fe0.1%Cr
[3] Zr1%Nb

Copyright © Advanced Nuclear Technology International Europe AB, ANT International, 2012.

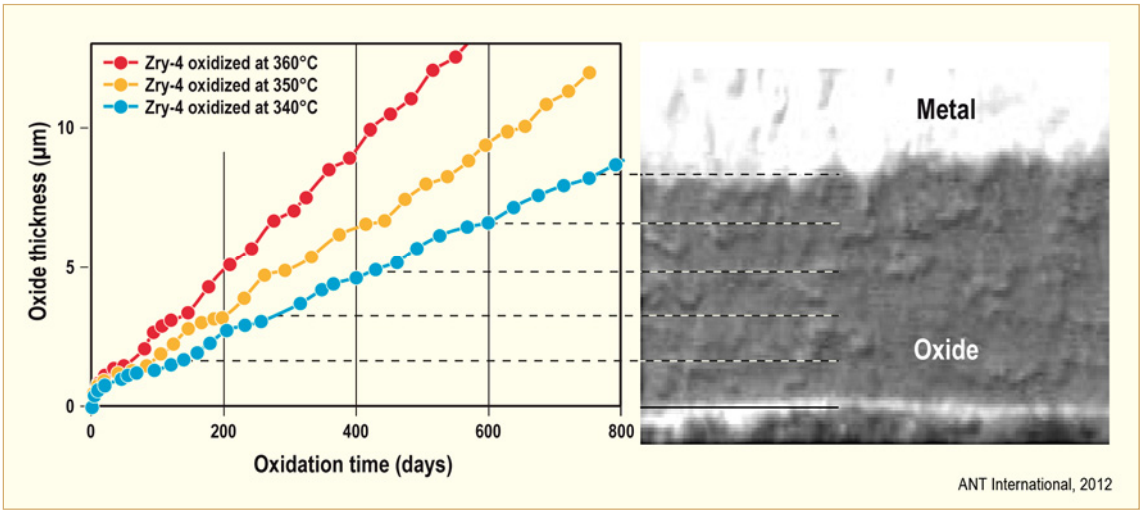

Figure 2-2: Corrosion of Zry-4 in autoclave at 340-360°C, after [Bonieau et al, 2007].

Several models, to predict the PWR fuel cladding corrosion behaviour, have been proposed over the years. Some of them are listed in Table 2-1 together with the information on the basic concept and the most important parameters, such as the used corrosion rate constants and activation temperatures for the pre- and post-transition range, the transition thickness, as well as the applied thermal conductivity of the oxide layer. Most models assume that there is an initial period where corrosion is similar as that out reactor and that corrosion rate is only increased above a certain in-PWR transition thickness, which varies between 2 and 6 µm. In the following the important parameters will be discussed.

Many models consider several other parameters, in addition to temperature having an impact on corrosion rate. Most other parameters are taken into account in the Electric Power Research Institute (EPRI) PFCC code. For pre transition corrosion behaviour, only the potential effects of Li and of a very low SPP size, was considered in the equation:

Eq. 2-4: $$ds^3/dt = C_1 \cdot \exp(-Q/R/T) \cdot F_{Li1} \cdot [1+F_{Fe}]$$

and $$t_{trans} = S_{trans}^3/(ds/dt)$$

where

t = time in days,

s = oxide thickness in µm, S_{trans} = 2 µm,

C_1 = an experimental constant = 5.8876 • E10 $\mu m^3/d$,

Q_1/R = an activation temperature = 16950 K,

T = the oxide/metal interface temperature in K,

F_{Li1} = a lithium factor deteriorating the oxide protectiveness, and F_{Fe} = a SPP dissolution term, see Sections 2.3 and 2.6.1 for more details.

Copyright © Advanced Nuclear Technology International Europe AB, ANT International, 2012.

For post transition corrosion behaviour the separate effects of Li, Tin content of the cladding, heat flux, radial hydrogen distribution, SPP dissolution, and oxide radiation damage effect are considered in the EPRI PFCC code by the following correlation:

Eq. 2-5: $ds/dt = C_2 \cdot \exp(-Q/RT) \cdot F_{Li} \cdot F_{Sn} \cdot F_{QQ} \cdot [1+F_{H2}+F_{Fe}+F_{\varphi}]$

where

s = oxide thickness in μm,

t = time in days,

C_2 = post-transition rate constant, taken equal to 8.198E6 μm/d (for hydrogen content less than 400 ppm),

Q_2/R = activation temperature, 12500 K (for hydrogen content less than 400 ppm),

T = metal-oxide interface temperature, K,

F_{Li} = lithium hydroxide corrosion enhancement factor,

F_{Sn} = tin content corrosion enhancement factor, see Sections 2.3 and 2.6.1 for more details,

F_{QQ} = heat flux (QQ) enhancement factor, see Sections 2.3 and 2.6.1 for more details,

F_{H2} = hydrogen radial redistribution corrosion enhancement factor, see Sections 2.3 and 2.6.1 for more details,

F_{Fe} = precipitate irradiation dissolution effect corrosion enhancement factor, see Sections 2.3 and 2.6.1 for more details,

F_{φ} = oxide radiation damage effect corrosion enhancement factor, see Sections 2.3 and 2.6.1 for more details.

The metal-oxide interface temperature, *T*, is calculated in the EPRI PFCC code from the single channel model-determined cladding wall temperature using 1.5 W/(m·K) for the thermal conductivity of zirconium oxide (ZrO_2).

Obviously there are quite different models for analysis and prediction of in-PWR corrosion behaviour of Zr alloys. It will be shown in the next sections that the state of knowledge is not good enough to judge on the correctness of all the different models. However, it has to be pointed out that conclusion from analysis with a particular model cannot be compared to conclusions derived with another model. For this report it was decided to apply the Siemens model with its particular corrosion constants (as default constants), because it allows comparison with the particular corrosion constants (enhancement factors) of the largest published data base for very different material composition and final heat treatment conditions.

Copyright © Advanced Nuclear Technology International Europe AB, ANT International, 2012.

Table 2-1: Basic concept, used corrosion rate constants, activation temperatures, transition thickness, and applied thermal conductivity of the oxide layer for different models to predict PWR Zry-4 cladding corrosion.

Model	Basic assumption on corrosion rate	Pretransition Q/R K	Pretransition Rate const (µm/d)	n	Transition at (µm)	Post transition Q/R K	Post transition Rate const (µm/d)	Thermal cond. of oxide layer W/(cm·K)	References
EPRI/KWU[4]/CE[5]	increases after transition depending on fast flux (for Zry-4)	16266	6.30E+09	3	2.2-2.4	13775	8.04E7+2.59E8 * (7.46E-15 * φ)$^{0.25}$	0.015	[Garzarolli et al, 1982a]
Siemens	is as out reactor up to transition and increases then by FF (~4 for Zry-4)	14200	1.50E+08	1	~5	14200	1.5E8*FF	0.015	[Garzarolli et al, 1985a,1993,1996a]
Advanced Nuclear Fuel (ANF)	1978 MATPRO model, increases by temperature dependent A and independent E	15660	4.97E+9*A	3	1.3–1.9	14080	8.288E+7*A*E	0.0173	[Van Swam & Shann, 1991]
British Nuclear Fuels Limited (BNFL)	increases after transition by FF, depending on fast flux and material, Recrystallized (RX)-degree, H-content, Li-content	16250	5.07E+13	3	2.2	14172	1.5E8*FF	0.015 at <48 µm 0.008 at >65 µm	[Polley et al, 1992]
ABB	increases linearly with fast flux and the oxide thickness >6 µm	16260	1.34E+10	3	2.3-2.6	13775	1.04E8* (1+F · φ · (Sox-6)	0.022	[Forsberg et al, 1995]
EPRI-PFCC	increases after transition depending on fast flux, Fe-cont., Sn-cont., SPP-size, H-cont., Li-cont..	16952	5.88E+10	3	2	12500 at <400 ppmH 4600 at 18800 ppmH	C · φ$^{0.25}$	0.015	[Levy et al, 1995] [Cheng et al, 1996]
CEA[6]/EDF[7]/ FRAMATOME	follows repeated transition and increases in PWR after transition to ≈2 and >18 µm to≈5 (for Zry-4)	16000	6.92E+09	3	1.75 for Zry-4 2.08, M2	16000		0.022 (>18 µm 0.008)	[Pêcheur et al, 2004]
φ = fast neutron flux in n/cm²-s, F or FF = fitting factor, Sox = oxide thickness, A=120*exp(-0.0071*T), E = temperature independent multiplication factor									
ANT International, 2012									

[4] KraftwerkUnion
[5] Combustion Engineering
[6] Commissariat à l'Energie Atomique
[7] Electricité de France

Copyright © Advanced Nuclear Technology International Europe AB, ANT International, 2012.

3 Corrosion modelling

3.1 Important PWR FA data

There are a wide variety of different types of FAs for PWR, e.g. from 14x14 to 18x18. Figure 3-1 shows a typical PWR FA. In this figure all the different FA components are shown and the material selections for these components are provided too.

As far as the FR diameter is concerned one can separate the PWR FA designs with thick (~11 mm) and with thin FRs (~9.5 mm). FA designs with thick rods are the:

- 14x14 and 15x15 FAs for Westinghouse Type PWRs,
- 15x15 (Mark B) FAs for B&W PWRs,
- 14x14 FAs for CE PWRs and
- 15x15 and 16x16 FAs for Siemens PWRs.

FA designs with thin rods are the:

- 17x17 FAs for Westinghouse Type PWRs,
- 17x17 (Mark C) FAs for B&W PWRs,
- 16x16 FAs for CE PWRs and
- 18x18 FAs for Siemens PWRs.

The pitch[9] between the individual FRs is about 1.33 times larger than the FR diameter and the average distance between the outer rows of neighbouring assemblies is about 1 mm larger than the distance between internal rods.

Each FA contains 16-25 GTs with an OD about 1.28 times larger than the FR diameter. Only in case of the CE-FAs there are only 5 thicker GTs replacing 4 FRs per GT.

[9] distance between the centre of two adjacent rods

Copyright © Advanced Nuclear Technology International Europe AB, ANT International, 2012.

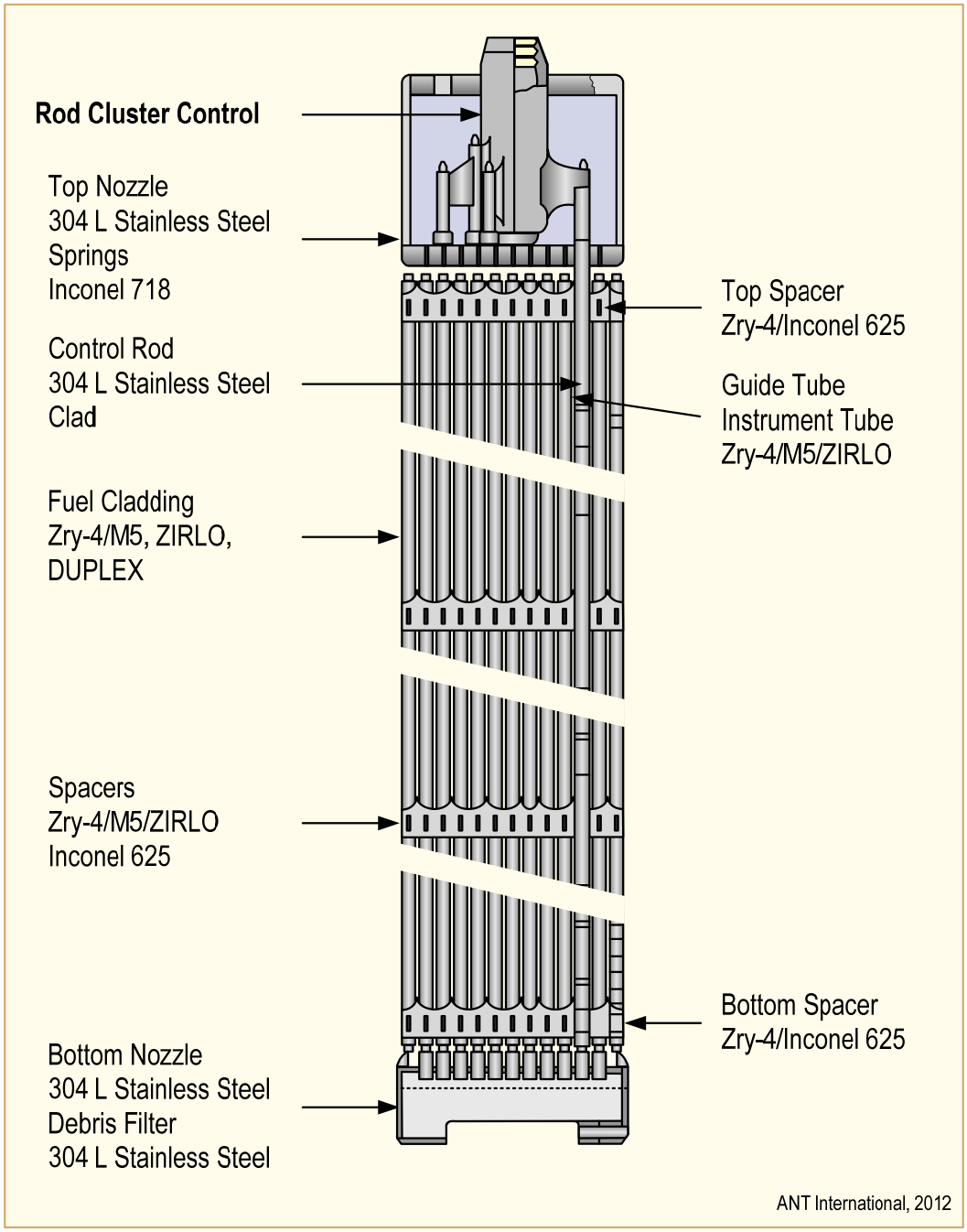

Figure 3-1: Typical PWR FA [Cox et al, 2005].

Around each FR4, potentially different, sub-channels exist for the coolant flow. The different types of sub-channels present in a PWR FA are illustrated in Figure 3-2. It can be seen that the sub-channel size varies depending on the proximity of the FR to other FRs, GTs or water gaps. Ideally the FRs can be subdivided into several categories, depending on the neighbouring FRs and the neighbouring sub-channels, in:

- Internal FRs with only FRs as nearest neighbours, (FR position 0),
- internal FRs with FRs and 1, 2 or 3 GTs as nearest neighbours. (FR position 1, 2 and 3),
- peripheral FRs (FR position 4),
- corner rod (FR position 5),

Copyright © Advanced Nuclear Technology International Europe AB, ANT International, 2012.

- and as a special case peripheral FRs with oxide measurements only at the outer periphery (Measurements of outer rods by line scans within an assembly, FR position 6).

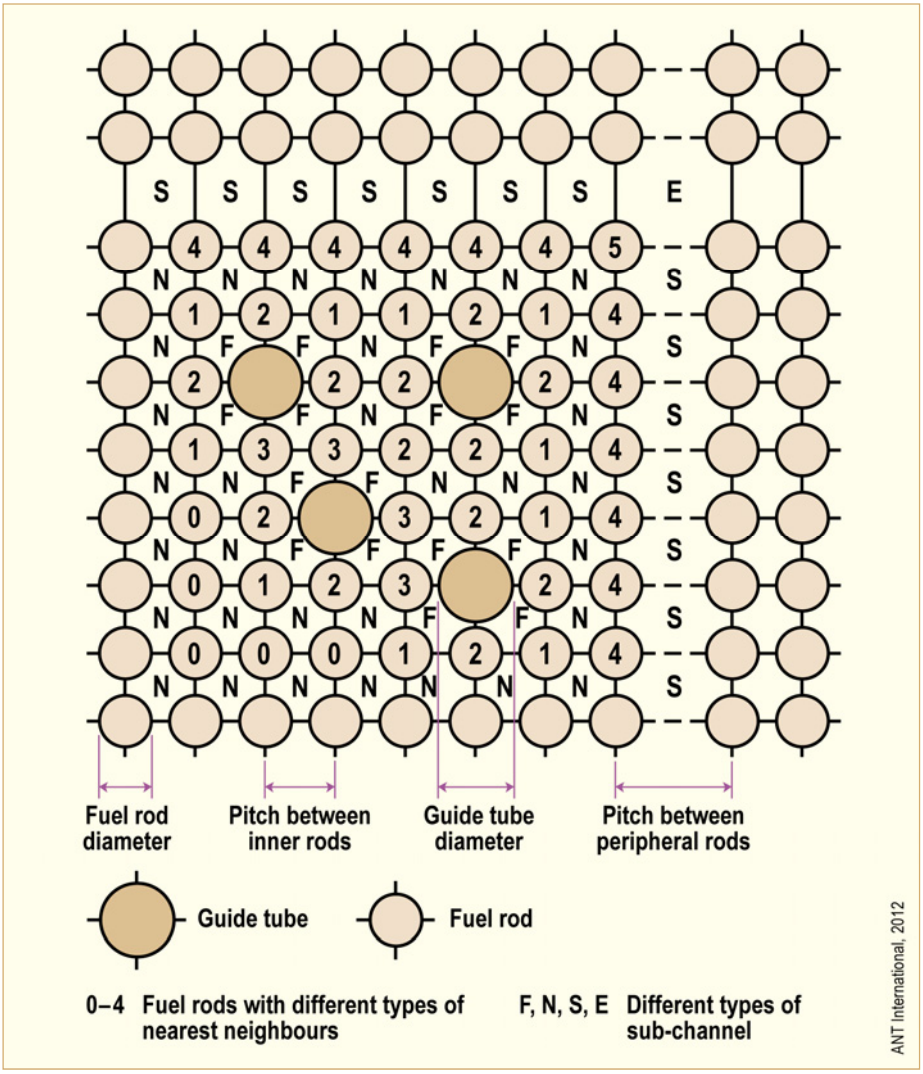

Figure 3-2: Differences in sub-channel geometry within the core illustrated by a part of a FA, after [Garzarolli et al, 1982a].

The important data that are needed for a PWR cladding corrosion model are:

1) Reactor Fuel Data as the:
   - Reactor name,
   - No. of FRs per FA side (***type***, e.g. 14 for a 14x14 FA or 18 for a 18x18 FA),
   - No. of GTs per FA (***ngt***, e.g. 17 or 25),
   - active length in mm (e.g. 2440 or 4200 mm),
   - FR length in mm (2680 or 4490 mm),
   - length of the lower plenum in mm (e.g. 0 or 317 mm),
   - FR diameter in mm (***dfr***, e.g. 9.3 or 10.75 mm),
   - outer GT diameter in mm (***dgt***, e.g. 12.2 or 13.8 mm),
   - FR pitch in mm (***pfr***, e.g. 12.6 or 14.9 mm),
   - weight of uranium per unit FR length in g/cm (e.g. 4.7 or 5.8),

Copyright © Advanced Nuclear Technology International Europe AB, ANT International, 2012.

4 Evaluation of literature data with Matthias 1

The evaluation of published oxide thickness profiles and oxide peak values of different FRs was done by use of the developed analysis program Matthias-I. For these analysis the reactor data, FR data, power history data, oxide thickness data for a given number of axial positions and cycles, and axial power shapes are input in the this analysis program (see Manual in Appendix A.1). After the start of calculation, the calculated results are exported to an EXCEL sheet (the LocalHeatFlux, SteamingRate, alpha_infinite, alpha_x, OxideLayerFF1, OxideLayerFF, Measured_OxideLayer, NormalizedTime, Parttime, FittingFactor, Tox_beg., Tox_end, and InputData). These data are then used for;

- After the "start of calculation", the calculated results are "exported to an EXCEL sheet". In this EXCEL sheet the LocalHeatFlux, SteamingRate, alpha_infinite, alpha_x, OxideLayerFF1, OxideLayerFF, Measured_OxideLayer, NormalizedTime, Parttime, FittingFactor, Tox_beg., Tox_end, and InputData are given on separate pages. These data can then be used for the final analysis which may be: evaluation of the oxide growth rate in comparison to the corrosion characteristics of Zry-4 out-of- reactor (oxide thickness versus normalized time plot),
- calculating the corrosion enhancement factor after the transition (e.g. 5 µm) as function of axial position,
- calculating the average metal-oxide interface temperature, that can be deduced for the last cycle or part of a last cycle, by averaging the Tox_beg. and Tox_end. values during this period for the given axial positions.

By:

- Checking the steaming rate history for the given axial positions,
- comparing the oxide layer thickness with the critical oxide layer thickness resulting in a hydrogen content of ≥300 ppm and,
- evaluating the LocalHeatFlux data to assess whether the heat flux was ≥50 W/cm² or not during the last irradiation period.

It can be assessed if any corrosion enhancement due to boiling or hydride rim formation can be expected. For the analysis provided in Section 4, several input data have been used. The used reactor data, FR data, and power history data are given in Appendix B and the axial profiles in Appendix C.

Copyright © Advanced Nuclear Technology International Europe AB, ANT International, 2012.

4.1 Evaluation of published oxide profiles from Zry-4 FRs with different BUs, with and without hydride rims varying also the basic corrosion constants (adjust parameters).

The oxide thickness of Low-Sn-Zry-4 claddings often exhibits a local increase in the upper range of the FR due to the formation of a dense hydride rim, as reported in Section 2.6.1. Such a localized increased corrosion rate has been shown in Figure 2-42. [Seibold et al, 1995] reported that the oxide layer profile of the "Konvoi" FR H4 with a low Sn Zry-4 cladding at an elevation of 2300 to 4000mm was increased due to a hydride rim. It was further reported that this hydride rim was formed during the 2nd cycle of operation at a rather high rod power if oxide thickness exceeded 20 to 25 µm. The increased corrosion rate continued into the third cycle although the rod power was low. The analysis of these oxide thickness profiles with the oxide analysis model Matthias-I for three different onset values of 0, 2, and 5 µm, when in-PWR corrosion increase ($S_{ox}tr$) occurs are shown in Figure 4-1. For the analysis the reactor data, FR data, power history data given in Table B-1 and the axial profile "Generic-actL3900.exp" (Table C-1) were applied. The Figure 4-1d shows that corrosion enhancement (F) is different in the axial range with normal corrosion (below 2300 mm and above 4000 mm) and in the range with a hydride rim affected corrosion (between 2300 and 4000 mm). The deduced enhancement factor (F) of the normal corrosion values increases with increasing oxide thickness at start of enhanced corrosion ($S_{ox}tr$), from 2.5 at a $S_{ox}tr$ of zero (Figure 4-1a), to 2.7 at a $S_{ox}tr$ of 2 µm (Figure 4-1b), and to 3.5 at a $S_{ox}tr$ of 5 µm (Figure 4-1c). Such changes of F can be expected considering similar modifications in Figure 3-6. The corrosion rate at the positions with a hydride rim is 6-7 times larger than the post transition corrosion rate of std. Zry-4 out of reactor (F), which means more than 2 times larger than the normal in-PWR corrosion rate.

Copyright © Advanced Nuclear Technology International Europe AB, ANT International, 2012.

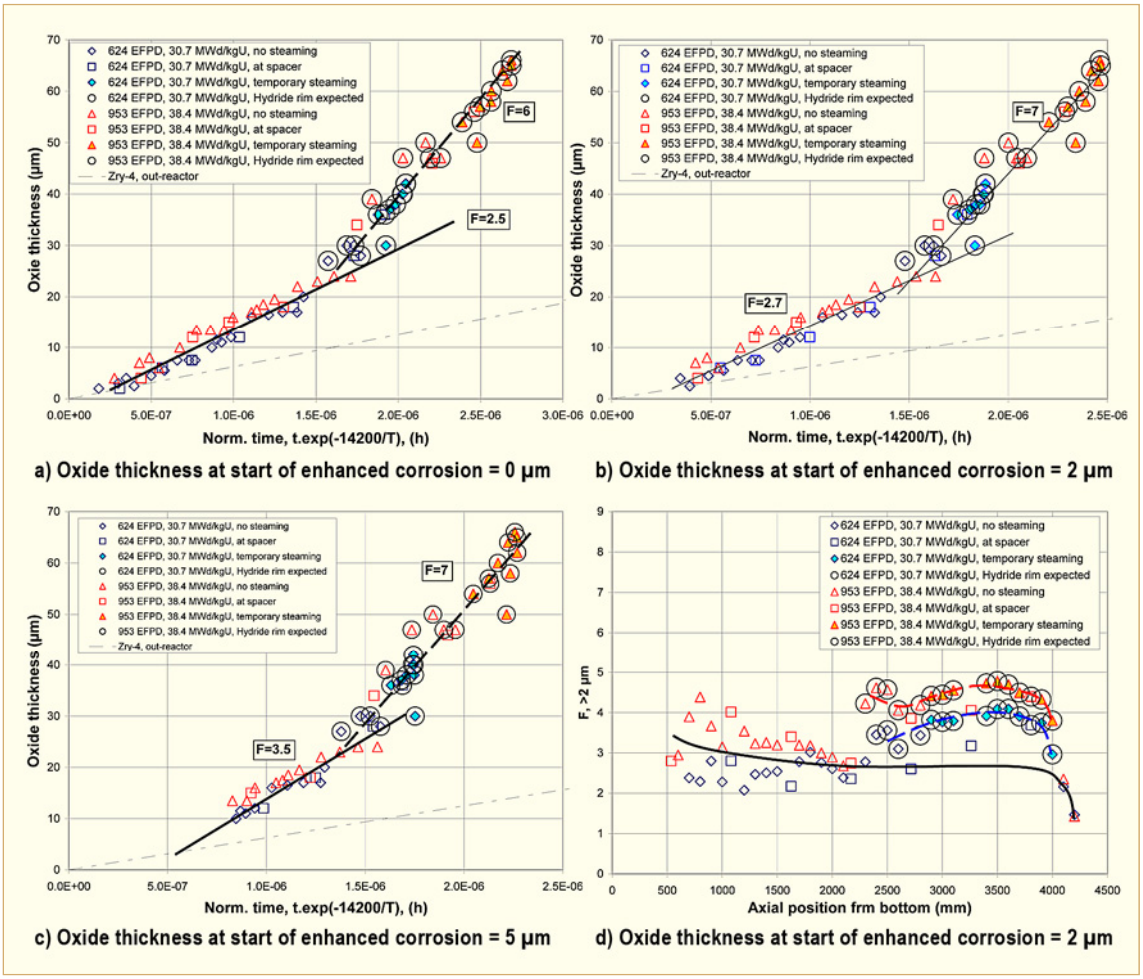

Figure 4-1: a)-c) Deduced Oxide Thickness versus Norm. Time assuming start of enhanced corrosion rate at 0, 2, and 5 µm. d) Corrosion enhancement factor, F, assuming that the start of enhanced corrosion occurs at 2 µm versus Axial Position from the reported oxide thickness profiles after 2 and 3 cycles of the Konvoi FR H4 with a low-Sn Zry-4 cladding [Seibold et al, 1995].

This rod suffered from the formation of a hydride rim by applying the default values (thermal conductivity of the oxide layer = 0.015 W/(cm·K), corrosion rate constant = 1.5E4 cm/d, and temperature dependency of corrosion rate of Q/R = 14200K) of the program Matthias-I.

The corrosion behaviour of Zry 4 with 1.53% Sn (Std.) and 1.22%Sn (Low-Sn) can be deduced from the oxide profiles reported by [Levy et al, 1995] and shown in Figure 4-2. The two FRs, 2804 and 2701, were irradiated in the Swiss PWR Gösgen at rather high duty conditions. The FR oxide thickness was measured after 2, 3, and 4 annual cycles at BUs of 29, 41 and 51 MWd/kgU, respectively. The FR cladding with 1.53% Sn showed larger oxide thickness values (max. 102 µm) than that of the FR with 1.22% Sn (max. 86 µm). The analysis of these oxide profiles was performed using the reactor data, FR data, power history data given in Table B-2 and the used axial profile "Generic-actL3658.exp" in Table C-2.

Copyright © Advanced Nuclear Technology International Europe AB, ANT International, 2012.

5 State of knowledge on in PWR Zr-Alloy corrosion kinetics

It has to be mentioned that the analyses performed in this report have some uncertainty, because the actual operation and thermal hydraulic data are not fully known so they have been estimated as good as possible. In most cases the PWRs were base load operated and the use of the EFPD as cycle length is relevant for FR oxidation analysis. However some of the PWRs, have been operated at a reduced power for long periods. In such cases the cycle length as well as the cycle power history (time steps of the axial profile) should include all periods with varying powers for an accurate analysis. For the calculations included in this report only a longer exposure time, but no power variations were considered for such cases. Furthermore, the oxide layer thickness was usually estimated by EC. EC, has however, shown a certain bias if compared with the more accurate thickness estimated by metallography in many cases. This bias results in a rather large uncertainty of the true oxide thickness, if the oxide thickness values are small, such as e.g. in the lower part of the FR or for low BUs rods. However, this uncertainty is much smaller for the upper part of high BU FR with larger oxide thickness. Thus only data from higher elevations and not too low BUs have been used for the correlations shown in the following.

Probably the largest published data base on corrosion behaviour of Zr alloys in PWR is from the extensive program of Siemens performed in the Swiss PWR Gösgen and several Vorkonvoi and Konvoi German PWRs. Similar assumptions were used for the analyses reported here by application of the default corrosion constants of the Matthias-I program.

From the analyzed oxide profiles it can be concluded that the corrosion of Zr-alloys depends on time (***t***) and exponential on temperature at the metal oxide interface (***T***) and can be reasonably described by:

Eq. 5-1: $$Normalized\ time = \Sigma\ t_i \bullet exp(-14200/T_i)$$

The analyzed oxide profiles have furthermore shown that there is always a critical oxide thickness at which corrosion rate is enhanced (Str). Above this critical value, the corrosion rate is increased (or decreased in comparison to the out-of-reactor corrosion rate of Zry-4) to a certain degree depending on material composition, material condition, and in some cases on BU. For most of the analyses performed in this report, Str was set to 5 µm. Besides this fast fluence corrosion enhancement occurring at an oxide thickness >5 µm there are several other potential causes that may increase corrosion rate above a certain oxide thickness or at a certain axial positions in addition, such as:

- Formation of a hydride rim,
- local steaming, which is considered to affect corrosion in the modified fuel duty Index,
- local temperature increase due to formation of a dense CRUD layer,
- steaming induced enrichment of Li in the outer porous layer above a critical concentration.

The hydride rim induced increase of corrosion rate was often seen among the analyzed oxide profiles. It was always noticed when the hydrogen pickup was larger than ~300 ppm and the surface heat flux at that moment was above of ~50 W/cm². The analyzed oxide profiles did not indicate any influence of steaming on the in-PWR corrosion rate. Weak indication of CRUD induced corrosion acceleration was seen in a few cases but Li increased corrosion rate was not seen, as expected.

The analyzed oxide profiles and peak oxide values of PWR FRs with Zry-4 claddings suggest that corrosion enhancement increases at high BUs. Such an enhancement was already reported by [Seibold & Garzarolli, 2002] for Zr-Sn-FeCr alloys and it was pointed out that the onset BU increased with decreasing Sn content.

Copyright © Advanced Nuclear Technology International Europe AB, ANT International, 2012.

Figure 5-1 shows the deduced F-values for:

- Rod positions which was not affected by spacers and/or hydride rims and with an oxide thickness > 5µm,
- the peak axial oxide values reported from experiments in Vandellos-II and Ohi-4.

Together with the trend curves of [Seibold & Garzarolli, 2002]. The figure shows a clear effect of BU which is somewhat delayed for low-Sn Zry-4 and a very good agreement between the new data from several PWRs, mostly Westinghouse-plants and the former trends from Siemens plants can be seen. Certainly, this does not necessary prove that in-PWR corrosion of Zry-4 increased at high BUs. The observed effect could certainly also be caused by a reduction of the thermal conductivity as for instance [Polley et al, 1992] assumes in his corrosion model. A disappearance of the BU effect on corrosion rate was also seen in this study by use of a very low thermal conductivity (0.005 instead of 0.015 W/(cm·K)) as shown in Figure 4-5c and d. Nevertheless, the analysis of FRs with Nb containing Zr alloys, such ZIRLO or MDA does not show a similar corrosion acceleration at high BU and is thus a strong argument against the thermal conductivity reduction theory.

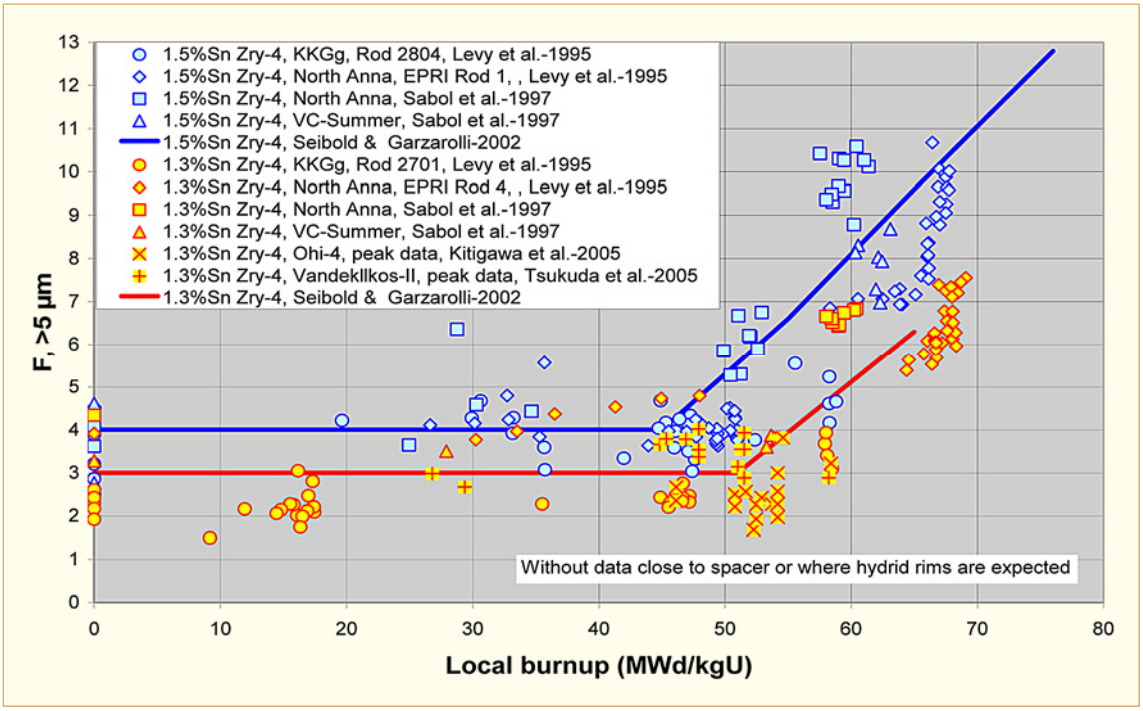

Figure 5-1: Effect of local BU on in-PWR corrosion enhancement of Zry-4 claddings at oxide thickness values > 5 µm.

[Bossis et al, 2006] explained the corrosion increase for Zry-4 claddings at high BUs (oxide layer thickness values) with by the formation of veins (Figure 5-2). His idea may well be the reason for the acceleration of corrosion enhancement of Zr-Sn-FeCr alloys at high BUs. The very wavy structure of the oxide/metal interface, usually observed for Zr-Sn-FeCr alloys, with a pronounced vein structure should be connected with an enrichment of the rather noble element Sn at metal/oxide interface positions that will be oxidized last Such local variations in the Sn content at the metal/oxide interface may cause quite large variations of the Zry creep strength [Adamson et al, 2009]. The easy oxidizing Nb will very likely not experience a similar displacement as Sn and because of its large effect on creep minimize any local variation of the creep strength.

The Nb containing alloy ZIRLO does not indicate any corrosion acceleration at high BU (Figure 5-3), at least up to 67 MWd/kgU. Also in case of MDA no acceleration is indicated up to 60 MWd/kgU, and in case of Low-Sn-ZIRLO, and M-MDA no corrosion enhancement can be noted at least up to 70 MWd/kgU (Figure 4-20 and Figure 4-22).

Copyright © Advanced Nuclear Technology International Europe AB, ANT International, 2012.

In addition to the high BU corrosion enhancement at high temperatures, shown in Figure 5-1 Zry-type alloys, which corrosion resistance is based on the number density, distribution, and size of $Zr(Fe,Cr)_2$ precipitates an other high BUs corrosion enhancement occurs at at surface temperatures below 330°C due to the irradiation induced dissolution of the precipitates, e.g. [Pêcheur et al, 1994] and [Seibold & Garzarolli, 2002]. This effect was not analyzed with Matthias-I considering that the oxide thickness values estimated by EC are not accurate enough for a reliable analysis of this effect.

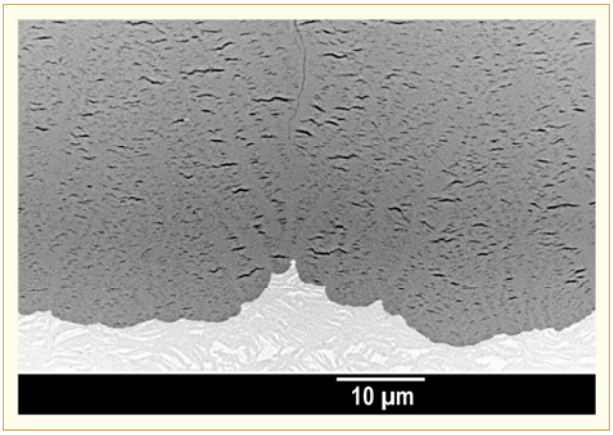

Figure 5-2: Cross section SEM micrograph, on s, in backscattered electron mode, of Zry-4 oxide layers formed in PWR after 6 cycles at span 6. Note the presence of radially distributed cracks free veins at a) macroscopic and b) microscopic levels and the correlation between the localization of radial cracks and these veins.

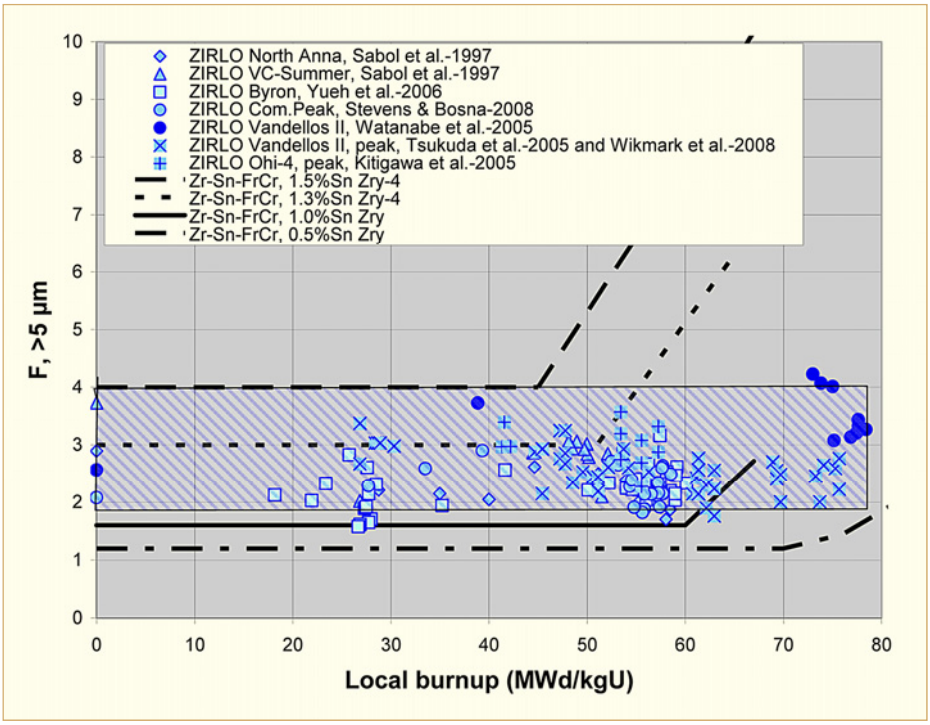

Figure 5-3: Effect of local BU on in-PWR corrosion enhancement of ZIRLO claddings at oxide thickness values > 5 µm.

Sn has a major effect on PWR corrosion even at BUs below 50 MWd/kgU, e.g. [Seibold & Gartzarolli, 2002]. The Sn-free FRs exhibit the lowest oxide layer thickness and alloys with highest Sn the highest. Figure 5-4 combines:

- The previously published results on in-PWR corrosion, [Seibold & Garzarolli, 2002],

Copyright © Advanced Nuclear Technology International Europe AB, ANT International, 2012.

7 References

Abe H. and Takeda K., *Development of advanced Zr alloy cladding tube (S2) for PWR*, Annual Meeting of the AESJ and private information, 2006.

Abram T. J., *Modelling the waterside corrosion of PWR fuel rods*, IAEA Technical Committee Meeting on Water Reactor Fuel Element Modelling at High Burnup, Windermere, 1994.

Adamson R., Cox B., Garzarolli F., Rudling P, Strasser A., and Wikmark G, *Corrosion of Zirconium Alloys*, ANT International, ZIRAT7 STR, 2002.

Adamson R. B, Garzarolli F. and Patterson C., *In-Reactor Creep of Zirconium Alloys*, ZIRAT14/IZNA9 Special Topical Report, ANT International, Mölnlycke, Sweden, 2009.

Adamson R. B, Garzarolli F., Patterson C., Rudling P. Strasser A. and Coleman K., *ZIRAT15/IZNA10 Annual Report*, ANT International, Mölnlycke, Sweden, 2010.

Arborelius J., Dahlbäck M., Hallstadius, L., Jourdain P., et al, *The Effect of Duplex Cladding Outer Component Tin Content on Corrosion Hydrogen Pick-up and Hydride Distribution at Very High Burnup*, 14th Int. Symposium on Zirconium in the Nuclear Industry, Stockholm, Sweden, p. 526, STP 1467, 2006.

Asher R. C. and Trowse F. W., *The Distribution of Hydrogen in Zirconium Alloy Fuel Cladding: The Effects of Heat Flux*, J. Nucl. Mat. 35, p. 115-121, 1970.

Beie H. J. et al, *Examination of the corrosion mechanism of Zr alloys*, ASTM STP 1245, pp. 615-643, 1994.

Besch O. A., Yagnik S. Y., Woods K. N., Eucken C. M. and Bradley E. R., *Corrosion behaviour of duplex and reference cladding in NPP Grohnde*, Zirconium in the Nuclear Industry: Eleventh International Symposium", ASTM STP 1295, Bradley E. R. and Sabol G. P., Eds. American Society for Testing and Materials, pp. 805-824, West Conshohocken, 1996.

Billot P., et al, *Development of a mechanistic model to assess the external corrosion of the Zry claddings in PWR*, ASTM STP 1023, pp. 165-184, 1989.

Billot, P. and Giordano A., *Comparison of Zircaloy corrosion models from the evaluation of m-reactor and out-of-pile loop performance*. Zirconium in the Nuclear Industry 9th Int. Symp., Kobe, ASTM-STP-1132, 539-565, 1991.

Billot P. et al, *Experimental and Theoretical Studies of Parameters that Influence Corrosion of Zircaloy-4*, ASTM STP 1245, pp. 351-377, 1994.

Blat M. and Noel D., *Detrimental Role of Hydrogen on the Corrosion Rate of Zirconium Alloys*, 11th Int. Symposium on Zirconium in the Nuclear Industry, Garmisch-Partenkirchen, Germany, p. 319, ASTM STP 1295, 1995.

Blat M., Legras, L., Noel, D., Amanrich, H., *Contribution to a Better Understanding of the Detrimental Role of Hydrogen on the corrosion Rate of Zircaloy-4 Cladding Materials*, 12th Int. Symposium on Zirconium in the Nuclear Industry, Toronto, Canada, p. 563, ASTM STP 1354, 1998.

Bonieau V. et al, *A New Model to predict the oxidation kinetics of Zr alloys in PWR*, 15th ASTM Internat. Symp. On Zr in the Nucl. Industry, Sunriver, Or. USA, 2007.

Bosma J. T. et al, *A Comprehensive Method for Assessing Fuel Performance Risks Due to Crud Deposition*, ANS LWR Fuel Performance Meeting, paper 1061, Orlando, Fl, 2004.

Bossis P. et al, *Comparison of the high burn-up corrosion on M5 and low tin Zircaloy-4*, ASTM STP 1467, pp. 494-524, 2006.

Copyright © Advanced Nuclear Technology International Europe AB, ANT International, 2012.

Bossis P. et al, *In PWR Comprehensive Study of High Burn-Up Corrosion and Growth Behaviour of M5 and Recrystallized Low-Tin Zircaloy-4,* Journal of ASTM International, Vol. 6, No. 2, Paper ID JAI101314, 2009.

Broy Y., Garzarolli F., Seibold A. and Van Swam L. F., *Influence of transition elements Fe, Cr, and V on long time corrosion in PWRs*, Zirconium in the Nuclear Industry: 12th Int'l Symposium, ASTM STP 1354, pp. 609-622, G. P. Sabol and G. D. Moan, Eds., West Conshohocken, PA, 2000.

Bryner J. S., *The cyclic nature of corrosion of Zircaloy-4 in 633K water*, J. Nucl. Mat., Vol. 82, pp. 84-101, 1979.

Chabretou V. et al, *Ultra low tin quaternary alloys PWR performance – Impact of tin content on corrosion and mechanical resistance*, 16th International ASTM Symposium on Zr in the Nuclear Industry, Chengdu, China, 2010.

Cheng B-C., Krüger R. M. and Adamson R. B., *Corrosion Behaviour of Irradiated Zircaloy*, Proc. 10th Int. Symp. in the Nucl. Ind., ASTM-STP-1245, pp. 400-418, 1994.

Cheng B. et al, *PWR Zircaloy fuel cladding corrosion performance, mechanisms, and modelling*, ASTM STP 1295, pp. 137-160, 1996.

Comstock R. J., Schoenberger G. and Sabol G. P., *Influence of Processing Variables and Alloy Chemistry on the Corrosion Behaviour of ZIRLO Nuclear Fuel Cladding*, Zirconium in the Nuclear Industry: 11th Int'l Symposium, ASTM STP 1295, E. R. Bradley and G. P. Sabol, Eds., American Society for Testing and Materials, pp. 710-725, 1996.

Cox B. and Johnston T., Corrosion V. 18, p.33, 1962.

Cox B. et al, *Waterside corrosion of zirconium alloys in nuclear power plants*, IAEA-TECDOC-996, 1998.

Cox B., Garzarolli F., Strasser A. and Rudling P., "Structural Behavior of Fuel and Fuel Channel Components", ZIRAT10/IZNA5 Special Topics Report, ANT International, Mölnlycke, Sweden, 2005.

Dalgaard S. B., *Long term corrosion and hydriding of Zry-4 fuel clad in commercial PWRs with forced convective heat transfer*, report at the Electrochemical Society, Inc. Washington, 1976.

Doriot S. et al, *Microstructural stability of M5 alloy irradiated up to high neutron fluences*, ASTM STP 1467, pp. 175-201, 2006.

Dyce I. H., *Corrosion of Zircaloy fuel cladding, the influence of heat flux*, Nulear Engeneering, pp. 253-255, 1964.

Etoh Y. and Shimada S., *Neutron Irradiation Effects on Intermetallic Precipitates in Zircaloy as a function of Fluence*, Journal of Nuclear Materials, Vol. 200, pp. 59-69, 1993.

[Evans E. and Polley V., *A review of the effect of Li on PWR fuel rod corrosion*, 6th Int. Conf. on Water chem. of Nucl, Rector Systems, BNES, Windermere, 1992

Forsberg K., Limbäck M., Massih A. R., A *model for uniform Zircaloy clad corrosion in pressurised water reactors*, Nuclear Engineering and Design, 154, 157-168, 1995.

Garde A. M., *Enhancement of Aqueous Corrosion of Zircaloy-4 Due to Hydride Precipitation at the Metal-Oxide Interface*, ASTM STP 1132, pp. 566-594, 1991.

Garzarolli F. et al, *Review of corrosion and dimensional behaviour of Zircaloy under water reactor conditions*, ASTM STP 681, pp. 91-106, 1979.

Copyright © Advanced Nuclear Technology International Europe AB, ANT International, 2012.

Garzarolli F. et al, *Review of PWR fuel rod waterside corrosion behaviour,* ERPR-Report, NP-1472, 1980.

Garzarolli F. et al, *Waterside corrosion of Zircaloy fuel rods*, ERPR-Report, NP-2789, 1982a.

Garzarolli F. et al, *Observation and analyses of the corrosion behaviour of PWR fuel*, ANS Topical Meeting on LWR Extended Burnup Fuel Performance and Utilization, Williamsburg, 1982b.

Garzarolli F. et al, *Progress in understanding PWR fuel rod waterside corrosion,* ANS Topical Meeting on Light Water Reactor Fuel Performance, Orlando, Fl., 1985a.

Garzarolli F. et al, *External cladding corrosion in water power reactors*, IAEA Techn. Comitte Meeting, CEN-Caderach, France, 1985b.

Garzarolli F., Steinberg E. and Weidinger H. G., *Microstructure and Corrosion Studies for Optimized PWR and BWR Zircaloy Cladding*, Zirconium in the Nuclear Industry, 8th Int'l Symposium, ASTM STP 1023, Van Swam L. F. P. and Eucken C. M., Eds., ASTM, Philadelphia, 202-212, 1989a.

Garzarolli F., Pohlmeyer J., Trapp-Pritsching S., Weidinger H.G., IAEA IWGFPT/34, Fundamental Aspects of Corrosion on Zirconium Base alloys in Water Reactor Environments, Vienna, pp. 65-72, 1989b.

Garzarolli F. et al, *Effects of high neutron fluences on microstructure and growth of Zircaloy-4*, ASTM STP 1023pp. 641-657, 1989c.

Garzarolli F and Goll W., *Review on measurements of thermal conductivity of oxide layers*, Halden Workshop on Zircaloy Corrosion and Hydriding, 15. October 1993.

Garzarolli F et al, *Accelerated Corrosion at High Burnups, Proposal for an Examination Programme*, Halden Workshop on Zircaloy Corrosion and Hydriding, 15. October 1993.

Garzarolli F., Stehle H., Steinberg, E., *Behavior and Properties of Zircaloys in Power Reactors: A Short Review of Pertinent Aspects in LWR Fuel*, Zirconium in the Nuclear Industry: 11th Int'l Symposium, ASTM STP 1295, Bradley E. R. and Sabol G. P., Eds., American Society for Testing and Materials, 12-32, 1996a.

Garzarolli F., Broy Y. and Busch R. A., *Comparison of the Long-Time Corrosion Behavior of Certain Zr Alloys in PWR, BWR, and Laboratory Tests*, Zirconium in the Nuclear Industry: 11th Int'l Symposium, ASTM STP 1295, Bradley E. R. and Sabol G. P., Eds., ASTM, 850-864, 1996b.

Garzarolli F. et al, *Means to avoid unusually increased PWR fuel rod corrosion*, 24 Annual Meeting Sociedad Nuclear Espanola, Valladolid, 1998.

Garzarolli F., *Improvements in Zirconium Alloys for PWR and BWR Fuel Materials and Plans for the Future*, ZIRAT4 Meeting, New York, USA, Jan. 2000.

Garzarolli F. et al, *Corrosion phenomena at high burnup*, 10th Environmental Degradation Conference, Lake Tahoe, Nevada, 2001.

Garzarolli F. et al, *Alternative Zr alloys with irradiation resistant precipitates for high burnup application*, ASTM STP 1423, pp.119-132, 2002a.

Garzarolli F., Sell H.-J., and Thomazet J., *PWR Li coolant chemistry and fuel cladding performance*, Jahrestagung Kerntechnik, 2002b.

Garzarolli F. et al, *Alternative Zr alloys with irradiation resistant precipitates for high burnup BWR application*, ASTM-STP 1423, pp. 119-132, 2002c.

Copyright © Advanced Nuclear Technology International Europe AB, ANT International, 2012.

Appendix A – User manual for the attached computer Software

Two different computer programs were developed for this report:

- An Oxide Data Analysis Model, Matthias-I and.
- An Oxide Thickness Prediction Model, Matthias-II.

Both programs were written with Microsoft Visual Basic 2010 Express. The source code was compiled to an executable version for the two programs. A CD-Rom with the two executable programs Matthias I and Matthias II is attached to the report.

A.1 Oxide data analysis model, Matthias-I

After the start of the **"Oxide Data Analysis Model", Matthias-I** program the "**Enter Data" button** has to clicked upon. Then the characteristic FR data have to be inserted in the **Reactor Fuel Data** table such as:

Reactor name	a string with a range of 1-30
FRs per FA side	an integer with a range of 1-20
GTs per FA	an integer with a range of 0-25
Active length (mm)	a float with a range of 100-4000
Total FR length (mm)	a float with a range of 100-4000
Lower plenum (mm)	a float with a range of 0-400
FR-diameter (mm)	a float with a range of 8.5-12.5
GT-diameter (mm)	a float with a range of 10-18
FR-pitch (mm)	a float with a range of 10-16
FA-pitch (mm)	a float with a range of 1-300
U-length-weight (g/cm)	a float with a range of 2-7
Number of spacers	an integer with a range of 0-20
Number of mixing-grids	an integer with a range of 0-20
Height of spacer grid	a float with a range of 0-60
Height of mixing grid	a float with a range of 0-60
	ANT International, 2012

Furthermore the axial position of the upper end of each spacer grid and if exist mixing grid has to be entered in mm. The data can be saved, or if already saved previously, the data can be loaded.

Copyright © Advanced Nuclear Technology International Europe AB, ANT International, 2012.

Then the **FR and Oxide Data latch** has to be opened, containing three different tables. In the table on the left side **General FR information** have to be input, such as:

Reactor name	a string with a range of 1-30
FA name	a string with a range of 1-30
FR name	a string with a range of 1-30
Cladding	a string with a range of 1-30
Lot	a string with a range of 1-30
Number of cycles	an integer with a range of 1-30
Number of axial positions	an integer with a range of 1-100

ANT International, 2012

In the table in the upper part of the right side the **Fuel operation information** have to be input for each FR exposure cycle, such as:

Name	cycle:1 cycle:2 cycle:n
FR-Pos.	integers with a range of 1-30
Cycle length (EFPD)	floats with a range of 1-2000
Core/Fuel-power ratio	floats with a range of 0.2-2
Tin (deg. C)	floats with a range of 220-330
Pressure (bar)	floats with a range of 120-170
Coolant flow (kg/FR-s)	floats with a range of 0.1-0.8
Rel. flow-rate	floats with a range of 0.2-2
FR-BU (MWd/kgU)	floats with a range of 0-150

ANT International, 2012

The number of cycles will entered automatically, as given in the General FR information table on the left side. The FR-Position is defined as shown in the FR-Pos Fields {0=internal FR with only FR neighbours, 1=internal FR with 1 GT neighbour, 2=internal FR with 2 GT neighbour, 3=internal FR with 3 GT neighbour, 4=peripheral FR, 5=corner rod, 6=peripheral FR with oxide measurement at the outer periphery (line scans)}

In the lower table on the right hand side **Oxide Data** have to be input for the number of axial positions and cycles defined in the General FR information table on the left side. For the number of positions the axial distance from bottom in mm (0-5000) have to be inserted. The oxide thickness values averaged around the circumference in µm (0-1000) have to be input for the different axial positions and cycles. For all positions and cycles where no data exist a “zero” (0) has to be entered. The data can be saved or if they have already been saved previously they can be loaded.

Copyright © Advanced Nuclear Technology International Europe AB, ANT International, 2012.

Afterwards the **Axial Profile latch** has to be opened and the **Time steps** per cycle and the **No of axial positions** have to be defined in the axial profile settings table.

Reactor name	a string with a range of 1-30
FA number	a string with a range of 1-30
Timesteps	an integer with a range of 1-30
No. of axial positions	an integer with a range of 10-100

ANT International, 2012

Then, for each time step of each cycle the relative duration (f 0.001-1) and relative power (0.5-2) has to be entered in the Axial Profile table in the lower part. For each axial power segment of each time step of each cycle, the relative axial power ((0.1-2) as deduced from core calculation or in core measurements has to be provided.

Name	"Cycle:1Time: 1" "Cycle:1Time: n" "Cycle:2Time: 1"
Relative duration	floats with a range of 0.001-1
Relative power	floats with a range of 0.5-2
Axial power of segment 1	floats with a range of 0.1-2
Axial power of segment 2	floats with a range of 0.1-2
Axial power of segment 3	floats with a range of 0.1-2
Axial power of segment 4	floats with a range of 0.1-2
Axial power of segment n	floats with a range of 0.1-2

ANT International, 2012

The data can be saved or if they have already saved previously they can be loaded.

Afterwards one has to go to the Matthias-I processing window and **Start Calculation.** After the calculation two buttons appear: 1) **Show Graphic** button**,** that opens a graphic showing an Oxide thickness versus Normalized time plot that compares the behaviour in the different cycles and 2) **Export to EXCEL** button, that open an EXCEL File containing the information on:

1) LocalHeatFlux (for each cycle, time step and axial position).
2) SteamingRate (for each cycle, time step and axial position).
3) Alpha_infinite (the alpha number not considering any grid for each cycle, time step and axial position).
4) Alpha_x the alpha number considering the entrance effects of the grids (for each cycle, time step and axial position).
5) OxideLayerFF1 (the oxide layer predicted for an enhancement factor of 1 for each cycle, time step and axial position).
6) OxideLayerFF (the oxide layer calculated with the deduced enhancement factor for the particular cycles and axial positions oxide data were put in).
7) Measured_OxideLayer (the values put in).
8) NormalizedTime (as calculated for each cycle, time step and axial position for the particular cycles oxide dada were put in).
9) Parttime (the time during a time step after that corrosion enhancement has started, as calculatd for each cycle, time step and axial position for the particular cycles oxide dada were put in).

Copyright © Advanced Nuclear Technology International Europe AB, ANT International, 2012.

Appendix B – Reactor-, FR-, and power history input data for analyzed oxide profiles

Table B-1: Konvoi FR H4 with a low Sn Zry-4 cladding.

Reactor data Reactor Konvoi		FR data Reactor Konvoi		Power history data			
FRs per side	18	FA name	C	**Cycle**	1	2	3
GTs per side	24	FR name	H4	**FR pos**	2	2	2
Active length (mm)	3900	Cladding	LT-Zry-4	**C length (mm)**	296	328	329
Total FR length (mm)	4830	Lot	nn	**Core/fuel power**	1.019	1.019	1.019
Lower plenum (mm)	317	No. of cycles	3	**Tin (°C)**	291.8	291.8	291.8
FR-dia. (mm)	9.5	No. ax. pos.	40	**Pressure (bar)**	158	158	158
GT-dia. (mm)	12.32			**Cool. flow (kg/FR-s)**	0.321	0.321	0.321
FR-pitch (mm)	12.7			**Rel. flow rate**	1	1	1
FA-pitch (mm)	230			**FR BU (MWd/kgU)**	15.04	30.7	38.4
ULW (kg/cm)	4.56						
Spacers	9						
Mixing grids	0						
ANT International, 2012							

Table B-2a: KKGg FRs 2804 and 2701 with Zry-4 claddings with 1.5 and 1.2% Sn.

Reactor data Reactor KKGg		FR data Reactor KKGg		Power history data				
FR 2804 with 1.5% Sn								
FRs per side	15	FA name	7-47	**Cycle**	1	2	3	4
GTs per side	20	FR name	28-04	**FR pos**	4	4	4	1
Active length (mm)	3400	Cladding	Zry-4	**C length (mm)**	325	298	309	303
Total FR length (mm)	3859	Lot	1.53%Sn	**Core/fuel power**	1.019	1.019	1.019	1.019
Lower plenum (mm)	257	No. of cycles	4	**Tin (°C)**	292.9	292.9	292.5	292
FR-dia. (mm)	10.75	No. ax. pos.	38	**Pressure (bar)**	155	155	155	155
GT-dia. (mm)	13.8			**Cool. flow (kg/FR-s)**	0.405	0.405	0.405	0.405
FR-pitch (mm)	14.3			**Rel. flow rate**	1	1	1	1
FA-pitch (mm)	215.6			**FR BU (MWd/kgU)**	14.7	29.4	41	51.1
ULW (kg/cm)	5.75							
Spacers	8							
Mixing grids	0							
ANT International, 2012								

Copyright © Advanced Nuclear Technology International Europe AB, ANT International, 2012.

Table B-2b: KKGg FRs 2804 and 2701 with Zry-4 claddings with 1.5 and 1.2% Sn.

Reactor data Reactor KKGg		FR data Reactor KKGg		Power history data				
FR 2701 with 1.2% Sn								
FRs per side	15	FA name	7-47	**Cycle**	1	2	3	4
GTs per side	20	FR name	27-01	**FR pos**	4	4	4	1
Active length (mm)	3400	Cladding	Zry-4	**C length (mm)**	325	298	309	303
Total FR length (mm)	3859	Lot	1.22%Sn	**Core/fuel power**	1.019	1.019	1.019	1.019
Lower plenum (mm)	257	No. of cycles	4	**Tin (°C)**	292.9	292.9	292.5	292
FR-dia. (mm)	10.75	No. ax. pos.	38	**Pressure (bar)**	155	155	155	155
GT-dia. (mm)	13.8			**Cool. Flow (kg/FR-s)**	0.405	0.405	0.405	0.405
FR-pitch (mm)	14.3			**Rel. flow rate**	1	1	1	1
FA-pitch (mm)	215.6			**FR BU (MWd/kgU)**	14.7	29.4	41	51.1
ULW (kg/cm)	5.75							
Spacers	8							
Mixing grids	0							
								ANT International, 2012

Table B-3: North Anna FRs with Zry-4 claddings as reported by [Levy et al, 1995]

Reactor data Reactor North Anna		FR data Reactor North Anna		Power history data				
FRs per FA side	17	FA name	F35	**Cycle**	1	2	3	4
GTs per FA side	25	FR name	1	**FR-pos**	4	4	4	4
Active length (mm)	3657	Cladding	Std. Zry-4	**Cycle length (days)**	372	370	418	516
Total FR length (mm)	3863	Lot	C	**Core/fuel-power ratio**	1.019	1.019	1.019	1.019
Lower plenum (mm)	0	FA-cycles	4	**Tin (°C)**	290.0	290.0	290.0	290.0
FR-diameter (mm)	9.5	No. axial pos.	58	**Pressure (bar)**	155	155	155	155
GT-diameter (mm)	12.24			**Coolant flow (kg/FR)**	0.338	0.338	0.338	0.338
FR-pitch (mm)	12.6			**Rel. flow rate**	1	1	1	1
FA-pitch (mm)	215.04			**FR BU (MWd/kgU)**	16.4	28.94	45.31	60.31
ULW (g/cm)	4.49							
No. of spacers grids	8							
No. of mixing-grids	0							
								ANT International, 2012

Copyright © Advanced Nuclear Technology International Europe AB, ANT International, 2012.

Table B-4: North Anna FRs with Zry-4 claddings as reported by [Comstock et al, 1996] and [Sabol et al, 1997].

Reactor data		**FR data**		**Power history data**			
Reactor North Anna		**Reactor North Anna**					
FRs per FA side	17	FA name	Test	**Cycle**	1	2	3
GTs per FA side	25	FR name	4	**FR pos**	4	4	4
Active length (mm)	3657	Cladding	Zry-4	**Cycle length (days)**	423	540	500
Total FR length (mm)	3863	Lot	nn	**Core/fuel-power ratio**	1.019	1.019	1.019
Lower plenum (mm)	0	No. of cycles	4	**Tin (°C)**	289.4	291.7	291.7
FR-diameter (mm)	9.5	No. axial pos.	29	**Pressure (bar)**	155	155	155
GT-diameter (mm)	12.24			**Coolant flow (kg/FR)**	0.338	0.338	0.338
FR-pitch (mm)	12.6			**Rel. flow rate**	1	1	1
FA-pitch (mm)	215.04			**FR BU (MWd/kgU)**	21.2	45.8	52.5
ULW (g/cm)	4.49						
No. of spacers-grids	8						
No. of mixing-grids	0						

ANT International, 2012

Table B-5: VC Summer FRs with Zry-4 claddings as reported by [Comstock et al, 1996] and [Sabol et al, 1997].

Reactor data		**FR data**		**Power history data**				
Reactor VC-Summer		**Reactor VC-Summer**						
FRs per FA side	17	FA name	Test	**Cycle**	1	2	3	4
GTs per FA	25	FR name	Test	**FR-pos**	4	4	4	4
Active length (mm)	3658	Cladding	Zry-4	**Cycle length (days)**	450	504	500	500
Total FR length (mm)	3852	Lot	nn	**Core/fuel-power ratio**	1.02	1.02	1.02	1.02
Lower plenum (mm)	0	No. of cycles	3	**Tin (°C)**	291	291	291	291
FR-diameter (mm)	9.14	No. axial pos	29	**Pressure (bar)**	158	158	158	158
GT-diameter (mm)	12.2			**Coolant flow (kg/FR)**	0.32	0.32	0.32	0.32
FR-pitch (mm)	12.6			**Rel. flow rate**	1	1	1	1
FA-pitch (mm)	215.04			**FR BU (MWd/kgU)**	24.1	42.2	56.1	59
ULW (g/cm)	4.2							
No. of spacers-grids	8							
No. of mixing-grids	3							

ANT International, 2012

Copyright © Advanced Nuclear Technology International Europe AB, ANT International, 2012.

Appendix C - Axial power profile

Table C-1: Axial power profile for Konvoi and Vorkonvoi PWRs (Generic-actL3900.exp).

		Cycle1		Cycle 2		Cycle 3-n	
		Time-1	Time-2	Time-1	Time-2	Time-1	Time-2
Rel. duration		**0.333**	**0.666**	**0.333**	**0.666**	**0.333**	**0.666**
Pel. power		**0.95**	**1.025**	**1.002**	**0.999**	**0.95**	**1.025**
1	63	0.3536	0.5412	0.3621	0.5549	0.411	0.6005
2	188.7	0.6254	0.806	0.6586	0.853	0.7088	0.9012
3	314.5	0.8267	0.973	0.8344	0.995	0.8516	1.0059
4	440.3	0.9771	1.072	0.9549	1.0697	0.9503	1.0562
5	566.1	1.0931	1.1313	1.0417	1.1089	1.0221	1.0831
6	691.9	1.177	1.1708	1.1055	1.1356	1.0778	1.1026
7	817.7	1.1937	1.1207	1.1181	1.0824	1.0935	1.0546
8	943.5	1.2054	1.1619	1.1303	1.1256	1.1059	1.0966
9	1069.4	1.2126	1.1186	1.1474	1.0885	1.1306	1.0671
10	1195.2	1.2312	1.1225	1.1641	1.0911	1.1491	1.0739
11	1321.0	1.0929	0.9748	1.0738	0.9758	1.0682	0.9669
12	1446.8	1.2414	1.1217	1.1778	1.0915	1.1613	1.0712
13	1572.6	1.2267	1.1003	1.1783	1.0789	1.1635	1.0603
14	1698.4	1.255	1.1314	1.223	1.1092	1.2103	1.0892
15	1824.2	1.1958	1.0752	1.1852	1.0708	1.1731	1.0528
16	1950.0	1.2066	1.0818	1.1902	1.0736	1.1823	1.0602
17	2075.8	1.2008	1.0808	1.1813	1.0712	1.1682	1.052
18	2201.6	1.2162	1.0896	1.1961	1.0817	1.1868	1.0667
19	2327.4	1.2018	1.0814	1.1825	1.0668	1.1687	1.0466
20	2453.2	1.1334	1.021	1.1385	1.0238	1.1356	1.0184
21	2579.0	1.1714	1.0681	1.1672	1.0599	1.1705	1.055
22	2704.8	1.1527	1.0676	1.1585	1.0616	1.1591	1.0554
23	2830.6	1.1317	1.0649	1.1478	1.0615	1.1443	1.0529
24	2956.5	1.0619	1.018	1.0769	1.0095	1.079	1.0101
25	3082.3	1.0717	1.0593	1.1044	1.0597	1.107	1.0601
26	3208.1	1.027	1.0522	1.0754	1.061	1.0792	1.0648
27	3333.9	0.9592	1.0283	1.0187	1.0423	1.0326	1.0587
28	3459.7	0.8358	0.9454	0.9097	0.9714	0.9319	0.9985
29	3585.5	0.7184	0.873	0.8047	0.9113	0.8355	0.9539
30	3711.3	0.5488	0.7213	0.6326	0.769	0.6791	0.8286
31	3837.1	0.3569	0.5478	0.4339	0.6097	0.5038	0.6952
							ANT International, 2012

Copyright © Advanced Nuclear Technology International Europe AB, ANT International, 2012.

Table C-2: Axial power profile for the PWR Gösgen (Generic-actL3658.exp)

		Cycle1		Cycle 2		Cycle 3-n	
		Time-1	Time-2	Time-1	Time-2	Time-1	Time-2
Rel. duration		**0.333**	**0.666**	**0.333**	**0.666**	**0.333**	**0.666**
Pel. power		**0.95**	**1.025**	**1.002**	**0.999**	**0.95**	**1.025**
1	59	0.3448	0.5324	0.3523	0.5448	0.4009	0.5901
2	177	0.6061	0.7896	0.6414	0.8388	0.6949	0.8906
3	295	0.7982	0.9515	0.8111	0.9779	0.8324	0.994
4	413	0.9574	1.0658	0.9402	1.0672	0.9386	1.0556
5	531	1.0525	1.1048	1.0113	1.0889	0.9962	1.0678
6	649	1.1645	1.1719	1.0955	1.1383	1.0686	1.1053
7	767	1.1955	1.1666	1.1212	1.13	1.0944	1.0986
8	885	1.2042	1.144	1.1286	1.107	1.105	1.0793
9	1003	1.1994	1.116	1.1279	1.0807	1.1063	1.0554
10	1121	1.2203	1.1202	1.1546	1.0897	1.1386	1.0701
11	1239	1.2344	1.122	1.1687	1.0912	1.1531	1.0726
12	1357	1.1757	1.0539	1.1366	1.04	1.1252	1.025
13	1475	1.2344	1.1133	1.1765	1.0865	1.1608	1.0671
14	1593	1.2059	1.0842	1.1829	1.0724	1.1714	1.0549
15	1711	1.1818	1.0604	1.1516	1.0477	1.1414	1.0326
16	1829	1.1966	1.0757	1.1811	1.0665	1.1713	1.051
17	1947	1.2041	1.0814	1.1863	1.0726	1.1761	1.0566
18	2065	1.2032	1.0704	1.1754	1.0607	1.1654	1.0451
19	2183	1.1654	1.0516	1.1598	1.0461	1.1535	1.0348
20	2301	1.0876	1.0323	1.1016	1.0251	1.1014	1.0221
21	2419	1.1544	1.0494	1.1549	1.0458	1.1555	1.0405
22	2537	1.1592	1.0677	1.1615	1.061	1.163	1.0552
23	2655	1.1413	1.0669	1.1534	1.0626	1.1514	1.0548
24	2773	0.9349	1.0174	0.9969	1.0325	1.0148	1.0535
25	2891	1.0735	1.0436	1.0968	1.0391	1.0995	1.0396
26	3009	1.0554	1.0575	1.095	1.0617	1.0969	1.0622
27	3127	1.0089	1.048	1.0617	1.0589	1.0679	1.0659
28	3245	0.8022	0.9192	0.8802	0.9493	0.9032	0.9777
29	3363	0.7034	0.8659	0.791	0.9056	0.8237	0.9515
30	3481	0.5307	0.7038	0.6139	0.7524	0.662	0.8134
31	3599	0.351	0.5425	0.4277	0.6049	0.4984	0.6912

ANT International, 2012

Copyright © Advanced Nuclear Technology International Europe AB, ANT International, 2012.

Appendix D – References

Abe H. and Takeda K., *Development of advanced Zr alloy cladding tube (S2) for PWR*, Annual Meeting of the AESJ and private information, 2006.

Arborelius J., Dahlbäck M., Hallstadius, L., Jourdain P., et al, *The Effect of Duplex Cladding Outer Component Tin Content on Corrosion Hydrogen Pick-up and Hydride Distribution at Very High Burnup*, 14th Int. Symposium on Zirconium in the Nuclear Industry, Stockholm, Sweden, p. 526, STP 1467, 2006.

Besch O. A., Yagnik S. Y., Woods K. N., Eucken C. M. and Bradley E. R., *Corrosion behaviour of duplex and reference cladding in NPP Grohnde*, Zirconium in the Nuclear Industry: Eleventh International Symposium", ASTM STP 1295, Bradley E. R. and Sabol G. P., Eds. American Society for Testing and Materials, pp. 805-824, West Conshohocken, 1996.

Chabretou V. et al, *Ultra low tin quaternary alloys PWR performance – Impact of tin content on corrosion and mechanical resistance*, 16th International ASTM Symposium on Zr in the Nuclear Industry, Chengdu, China, 2010.

Comstock R. J., Schoenberger G. and Sabol G. P., *Influence of Processing Variables and Alloy Chemistry on the Corrosion Behaviour of ZIRLO Nuclear Fuel Cladding*, Zirconium in the Nuclear Industry: 11th Int'l Symposium, ASTM STP 1295, E. R. Bradley and G. P. Sabol, Eds., American Society for Testing and Materials, pp. 710-725, 1996.

Levy S. et al, *EPRI PWR Fuel Cladding Corrosion, (PFCC) Model*, EPRI Report TR-105387-V2, December 1995.

Sasakawa T., Taniguchi Y., Murata T. and Sendo T., *Post-Irradiation Examination of Lead Use Assemblies for 55 GWD/T*, Proc. Water Reactor Fuel Performance Meeting, Kyoto, Japan, October, 2005.

Sabol G. P., Comstock R. J. Schoenberger G., Kunishi H. and Nuhfer D. L., *In-Reactor Fuel Cladding Corrosion Performance at Higher Burnups and Higher Coolant Temperatures*, Proceedings: International Topical Meeting on Light Water Fuel Performance, American Nuclear Society, pp. 397-404, Portland, OR, 1997.

Stevens J. and Bosma J., *Elevated RCS pH Program at Comanche Peak*, International Conference on Water Chemistry of Nuclear Reactor Systems, "NPC'08", Paper L2-3, Berlin, Germany, 2008.

Tsukuda Y et al, *Performance of advanced fuel materials for high burnup*, TopFuel 2003, Track 1, Würzburg Germany, 2003.

Watanabe S., Abeta S., Serna J., Alonso J. and Sendo T., Gonzalez, P., *Post irradiation examinations on 67-75 GWd/t rods for confirmation of the integrity and appropriate performance of the claddings for future*, Proc. Water Reactor Fuel Performance Meeting, Kyoto, Japan, October 2-6, 2005.

Wikmark G., Hallstadius L., and Yueh K., *Cladding to Sustain Corrosion, Creep and Growth at High Burnups*, Proceedings of 2008 Water Reactor Fuel Performance, paper 8077, Seoul, Korea, October 2008.

Yueh H. K., Kesterson R. L., Comstock R. J., Shah H. H., Colburn D. J., Dahlbäck M. and Hallstadius L., *Improved ZIRLOTM cladding performance through chemistry and process modifications*, Journal of ASTM International, 2, paper JAI12334, June 2005.

Copyright © Advanced Nuclear Technology International Europe AB, ANT International, 2012.